A Novel Underwater Acoustic Signal Denoising Algorithm for Gaussian/Non-Gaussian Impulsive Noise

Jingjing Wang, *Member, IEEE*, Jiaheng Li, Shefeng Yan, *Senior Member, IEEE*, Wei Shi, Xinghai Yang, *Member, IEEE*, Ying Guo, and T. Aaron Gulliver, *Senior Member, IEEE*

***Abstract*—Gaussian/non-Gaussian impulsive noises in underwater acoustic (UWA) channel seriously impact the quality of underwater acoustic communication. The common denoising algorithms are based on Gaussian noise model and are difficult to apply to the coexistence of Gaussian/non-Gaussian impulsive noises. Therefore, a new UWA noise model is described in this paper by combining the symmetric α-stable (SαS) distribution and normal distribution. Furthermore, a novel underwater acoustic signal denoising algorithm called AWMF+GDES is proposed. First, the non-Gaussian impulsive noise is adaptively suppressed by the adaptive window median filter (AWMF). Second, an enhanced wavelet threshold optimization algorithm with a new threshold function is proposed to suppress the Gaussian noise. The optimal threshold parameters are obtained based on good point set and dynamic elite group guidance combined simulated annealing selection artificial bee colony (GDES-ABC) algorithm. The numerical simulations demonstrate that the convergence speed and the convergence precision of the proposed GDES-ABC algorithm can be increased by 25%∼66% and 21%∼73%, respectively, compared with the existing algorithms. Finally, the experimental results verify the effectiveness of the proposed underwater acoustic signal denoising algorithm and demonstrate that both the proposed wavelet threshold optimization method based on GDES-ABC and the AWMF+GDES algorithm can obtain higher output signal-to-noise ratio (SNR), noise suppression ratio (NSR), and smaller root mean square error (RMSE) compared with the other algorithms.**

***Index Terms*—Gaussian/non-Gaussian noise, median filter, SαS, SNR, wavelet threshold optimization.**

I. Introduction

THE acoustic wave is widely used in the field of underwater communication because it is the only carrier that can realize underwater medium and long-distance transmission. However, in the process of underwater acoustic (UWA) communication, the complex marine environmental noise affects the acoustic signal leading to the degradation and distortion of the acoustic signal and the decline of the communication quality [1], [2].

According to the central limit theorem of statistics, the UWA noise can be described as the Gaussian noise. Therefore, most of the acoustic signal processing methods in underwater are based on Gaussian noise assumption. However, few sources will dominate on a particular range of frequency, which will contradict the central limit theorem by limiting the number of noise sources [3]. Moreover, the stochastic non-Gaussian impulsive noise exists in signals [4]–[6] and the probability density function (PDF) of UWA noise has a "heavier tail" than the Gaussian distribution. This will make the performance of the system sub-optimal or even worse when designed using Gaussian noise behavior. Therefore, it is essential to comprehensively investigate the UWA noise model.

Several models have been proposed in the literature for the PDF of UWA noise [3], [7]–[11], [14]. The Gaussian mixture model is widely used to characterize the UWA noise. However, it is unable to capture the heavier tail with a small number of Gaussian [3]. Compared with the Gaussian mixture model, the symmetric α-stable (SαS) distribution has "heavier tail" statistical characteristics of impulsive noise, which makes it consistent with the generation mechanism and the propagation conditions of the underwater impulsive noise [7]. Unfortunately, it has a limitation of not having a closed-form distribution except for $\alpha = 1, 2$ [3]. By describing the spacetime discipline of the noise source and the propagation characteristic of the noise, the parameters of the Middleton model possess physical meaning [11]. In practice, the UWA noise simultaneously suffers from the no-Gaussian impulsive noise and the Gaussian noise as shown in Fig. 1 [12], [13]. For this reason, it is difficult to determine several parameters with the Middleton model [14]. Therefore, this paper describes the combined noise model of UWA noise combining the SαS distribution and the normal distribution models. Furthermore, the energies of Gaussian noise and non-Gaussian impulsive noise are defined by SNR and mixed signal-to-noise ratio (MSNR), respectively.

The above-described non-Gaussian impulsive noise can be suppressed using the standard median filter (SMF). However,

Manuscript received June 11, 2020; revised October 9, 2020; accepted December 7, 2020. Date of publication December 16, 2020; date of current version February 12, 2021. This work was supported by the National Natural Science Foundation of China (NSFC) under Grants U1806201 and 61431020. The review of this paper was coordinated by Daniel Benevides da Costa. *(Corresponding authors: Jingjing Wang; Jiaheng Li.)*

Jingjing Wang, Jiaheng Li, Wei Shi, Xinghai Yang, and Ying Guo are with the School of Information Science and Technology, Qingdao University of Science and Technology, Qingdao 266061, China (e-mail: Kathy1003@163.com; lijiaheng1009@163.com; shiwei6670595@126.com; yangxh@qust.edu.cn; guoying@qust.edu.cn).

Shefeng Yan is with the Institute of Acoustics, Chinese Academy of Sciences, and the University of Chinese Academy of Sciences, Beijing 100190, China (e-mail: sfyan@ieee.org).

T. Aaron Gulliver is with the Department of Electrical and Computer Engineering, University of Victoria, Victoria, BCV8W2Y2, Canada (e-mail: agullive@ece.uvic.ca).

Digital Object Identifier 10.1109/TVT.2020.3044994

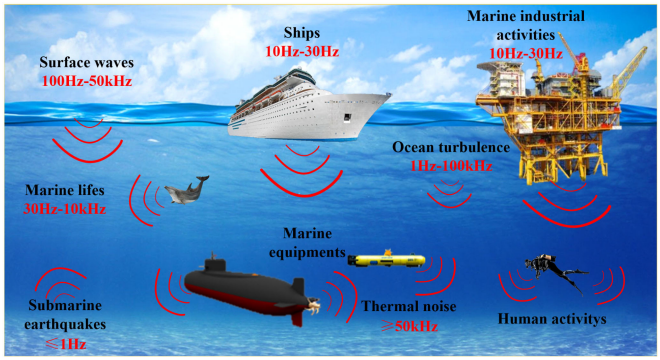

Fig. 1. Underwater anthropogenic and natural non-Gaussian impulsive noise sources.

the SMF processes the useful part of the received signal and distorts the signal of interest (SOI). To solve this problem, various improved filtering algorithms have been proposed [15], [16]. Vijaykumar *et al.* [17] proposed a fast switching based median-mean filter, using extreme minimum and maximum values to identify the noise and replaced it with median or mean value. Chanu *et al.* [18] proposed a two-stage switching vector median filter that detected the impulsive noise twice and replaced the noise with weighted vector median to suppress the impulsive noise while preserving the details of the SOI.

On the other hand, the Gaussian noise can be effectively suppressed using various existing methods such as filtering methods, wavelet transform (WT) methods, empirical mode decomposition (EMD) methods [19]–[21] and multistage singular spectrum analysis (MSSA) [22]. Among these methods, the wavelet threshold method is widely used because it can obtain the asymptotic optimal estimation of the SOI [23]–[25]. The threshold estimation and the construction of threshold function are the two key factors of the wavelet threshold method. Currently, the widely used threshold estimation method is the unified threshold estimation method proposed by Donoho and Johnstone *et al.* [26]–[28]. The unified threshold estimation method is based on the decision theory of multi-dimensional independent normal variables under the Gaussian noise model. Furthermore, the soft and hard threshold functions are designed to shrink the wavelet coefficients and obtain high denoising performance. However, the above-mentioned methods depend on the accurate estimation of noise variance and are difficult to apply to the actual unknown noise variance. Moreover, the above-mentioned methods shrink the wavelet coefficients according to a fixed structure, which lacks self-adaptability and reduces the flexibility of signal processing.

To overcome the above-described limitations, Yi *et al.* [29] proposed an improved threshold method based on Sigmoid function and discussed the effects of the types of wavelet basis functions, numbers of decomposition layers, threshold selection rules and threshold functions on the denoising performance. Sumithra *et al.* [30] proposed a trimmed thresholding method to achieve a compromise between the soft and the hard thresholding in order to effectively enhance the quality of the SOI in the background noise. Singh *et al.* [31] used the modulation channel selection as the threshold function and proposed a denoising method based on wavelet packet that was able to obtain a higher output SNR compared with other algorithms. Based on the improved thresholding function, Zhang *et al.* [32] proposed a dual-tree complex wavelet transform (ITF-DTCWT) denoising algorithm to ensure the approximate translation invariance and reduce the signal distortion.

In order to further improve the performance of wavelet threshold methods, various swarm intelligence optimization methods have been used to optimize the threshold parameters. Sun *et al.* [33] proposed a denoising scheme based on Shearlet transform and particle swarm optimization (PSO) algorithm. The scheme was able to efficiently eliminate the pseudo-Gibbs phenomenon and the noise. Bhutada *et al.* [34] optimized the adaptive threshold parameters based on PSO algorithm by minimizing the mean squared error (MSE) between the expected and the output signals. He *et al.* [35] proposed an improved threshold function based on a hyperbolic tangent function and minimized the MSE of reconstructed and expected signals using artificial fish swarm algorithm to obtain the optimal threshold parameters.

However, the above-mentioned swarm intelligence optimization algorithms still have some shortcomings, such as slow convergence and weakness of local refinement [36]–[38]. Kong *et al.* [39] proposed an improved artificial bee colony (ABC) algorithm based on elite group guidance and combined breadth-depth search strategy (ECABC) that was able to achieve high convergence precision in a short time. Based on three dynamic adjustment strategies to improve the optimization performance of PSO algorithm, Zhang *et al.* [40] proposed a parameter wavelet threshold signal denoising method (MPSO) to optimize the wavelet threshold parameters. The MSE between the reconstruct and the expected signals was used as the fitness function of the MPSO and both the SNR and the noise suppression ratio (NSR) of the output signal were effectively improved.

The actual underwater acoustic channel contains both Gaussian and non-Gaussian impulsive noises. Therefore, it is difficult to directly apply the above-mentioned denoising algorithms based on swarm intelligence optimization. First, it is difficult to construct the threshold function due to the lack of the general principle of establishing the threshold function. Second, the determination of threshold parameters is an iterative process that usually reaches the suboptimal value rather than the optimal value. Third, the increase in the number of iterations reduces the diversity of the population, which will make the above-mentioned algorithms fall into local optimum.

Therefore, this paper proposes a novel underwater acoustic signal denoising algorithm named AWMF+GDES, which is based on adaptive window median filter combined with wavelet threshold optimization. First, the Gaussian/non-Gaussian impulsive noises in the underwater acoustic channel are described by combining the SαS distribution and the normal distribution models. Then, an adaptive window median filter (AWMF) is proposed to suppress the non-Gaussian impulsive noise. Second, a new threshold function is designed based on the traditional wavelet threshold method to obtain the threshold parameters to be optimized. Then, the optimal threshold parameters are obtained using the GDES-ABC algorithm and the Gaussian

noise is suppressed. The main improvements of GDES-ABC algorithm include the population initialization based on good point set, neighborhood searching based on dynamic elite group, and simulated annealing selection mechanism.

The contributions of this paper are as follows:

- By combining the SαS distribution and the normal distribution, a new UWA noise model is described and the energies of Gaussian noise and non-Gaussian impulsive noise are defined by SNR and MSNR, respectively. Compared with the several existing models, the proposed model can capture a heavier tail with a small number of Gaussian and have a closed-form distribution for each α.
- According to the impulsive noise content, the AWMF adaptively changes the size of the filter window based on the proposed adaptive adjustment rule, which effectively balances the filtering performance and the computational complexity of the filter.
- To reduce the pseudo-Gibbs phenomenon, a new threshold function is designed and validated to improve the continuity and smoothness of the threshold shrinkage processing. Meanwhile, the GDES-ABC algorithm is utilized to obtain the optimal threshold parameters, which improves the estimation precision of the threshold parameters. The numerical simulations demonstrate that the proposed wavelet threshold optimization method can effectively reduce Gaussian noise.
- The three improvements of GDES-ABC algorithm are as follows: 1) The initial population is initialized based on the theory of good point set in order to ensure the averageness and the diversity of the population. 2) The random domain search method is replaced with the domain search method based on the dynamic elite group to accelerate the convergence speed and improve the search efficiency. 3) The domain selection based on simulated annealing mechanism is used to prevent the algorithm from falling into a local optimum. The numerical simulation results demonstrate that the convergence speed and the convergence precision of the GDES-ABC algorithm can be increased by 25%$\sim$66% and 21%$\sim$73%, respectively, compared with the existing algorithms.
- In this paper, the performance is examined in details and compared with the existing approaches using both simulated and real data. The numerical simulations and the experimental results demonstrate and validate that the proposed AWMF+GDES method can effectively improve the reception performance of underwater acoustic signals.

The rest of this paper is organized as follows. Section II introduces the system model. Section III describes the proposed underwater acoustic signal denoising algorithm. The effectiveness of the proposed algorithm is validated using simulated data and real data in Sections IV and V, respectively. Finally, Section VI concludes the paper.

II. System Model

For a single input single output (SISO) underwater acoustic communication system, the signal $y(t)$ received by receiver is described here in its digital form, as a set of discrete samples:

$$y(i) = s(i) + e(i), i = 1, 2, \ldots, N, \tag{1}$$

where $s(i)$ is the random SOI with random amplitude and phase; $e(i)$ is the additive background noise; and N is the total number of samples. The purpose of denoising is to recover the estimated signal $s'(i)$ of the SOI from $y(i)$ by using filters, WT, EMD or other signal processing methods, which would reduce the impact of $e(i)$ on the SOI.

The common denoising algorithms assume that the additive background noise in an underwater acoustic channel is a Gaussian noise source, and the PDF of the instantaneous intensity x of this source is:

$$f_{\mathrm{Gauss}}(x) = \frac{1}{\sqrt{2\pi}\sigma_e} e^{-\frac{x^2}{2\sigma_e^2}}. \tag{2}$$

The SNR is defined as:

$$\mathrm{SNR} = 10 \log \frac{\sigma_s^2}{\sigma_e^2}, \tag{3}$$

where σ_s^2 and σ_e^2 are the variances of the SOI and the additive white Gaussian noise (AWGN), respectively.

However, in the actual underwater acoustic channel, the PDFs of the non-Gaussian noise signal shown in Fig. 1 are similar to the Gaussian distribution. However, the tails are longer, and the probability of strong amplitude is higher, while the duration of those noise sources is shorter. The non-Gaussian noise has the characteristic of spike pulse that is regarded as a type of burst non-Gaussian impulsive signal. Therefore, it is difficult to apply the common denoising algorithms based on Gaussian model to the actual underwater acoustic channel.

The SαS distribution is a limit distribution model that satisfies the generalized central limit theorem, and can be consistent with the generation mechanism and propagation conditions of the above-mentioned non-Gaussian impulsive noise. Therefore, using the SαS distribution to describe the underwater spike impulsive noise has more advantages than the Gaussian distribution. If the characteristic function of a random variable X can be expressed as:

$$\varphi(x) = \exp\{jax - \gamma|x|^\alpha[1 + j\beta \mathrm{sgn}(x)\omega(x, \alpha)]\}, \tag{4}$$

where $j = \sqrt{-1}$, a is the local paremeter and $-\infty < a < \infty$, and

$$\omega(x, \alpha) = \begin{cases} \tan(\frac{\alpha\pi}{2}), \alpha \neq 1 \\ \frac{2}{\pi} \log|x|, \alpha = 1 \end{cases}, \tag{5}$$

$$\mathrm{sgn}(x) = \begin{cases} 1, x > 0 \\ 0, x = 0 \\ -1, x < 0 \end{cases}. \tag{6}$$

Then, the random variable X satisfies the α stable distribution. Where α is the characteristic exponent that determines the degree of pulse characteristics of the distribution and $0 < \alpha \leq 2$. The bigger the α is, the more obvious the pulse characteristic will be. When $\alpha = 2$, the α stable distribution is equivalent to Gaussian distribution. β is the symmetric parameter that is used to determine the slope of the distribution and $-1 \leq \beta \leq 1$. γ is

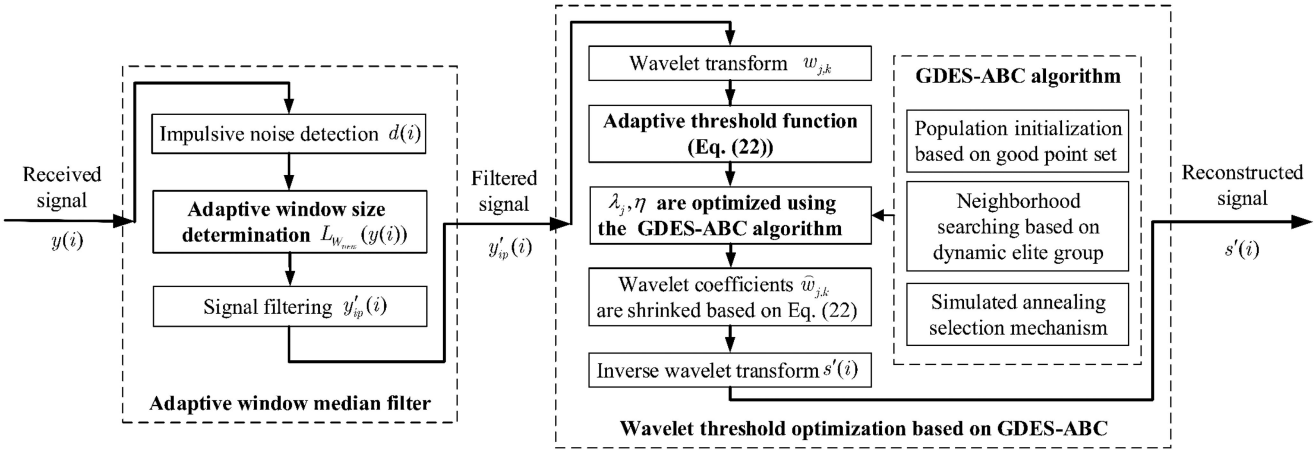

Fig. 2. Process of the processed scheme.

the dispersion of the distribution and $\gamma > 0$, which is similar to the variance of Gaussian distribution.

When $\beta = 0$, Eq. (4) can be written as:

$$\varphi(x) = \exp(jax - \gamma|x|^{\alpha}). \tag{7}$$

In this case, the distribution is called the SαS distribution, recorded as $X \sim \mathrm{S}\alpha\mathrm{S}$. For simplicity, the local parameter a is assumed to be 0. Then, the PDF of the SαS distribution is:

$$f_{\mathrm{S}\alpha\mathrm{S}}(\gamma, x) = \frac{1}{2\pi}\int_{-\infty}^{\infty} \exp(-\gamma|\omega|^{\alpha})\mathrm{e}^{-j\omega x} d\omega. \tag{8}$$

It is impossible to calculate the variance of non-Gaussian impulsive noise satisfied with the SαS distribution. Therefore, the MSNR is used to describe the power of non-Gaussian impulsive noise. The MSNR is defined as:

$$\mathrm{MSNR} = 10\log\left(\frac{\sigma_{\mathrm{s}}^2}{\gamma}\right), \tag{9}$$

where σ_s^2 and γ are the variance of the SOI and the dispersion of non-Gaussian impulsive noise satisfied with the SαS distribution, respectively.

To more realistically describe the noise in the real environment, it is assumed that the underwater acoustic noise is obtained by the superposition of Gaussian noise and non-Gaussian impulsive noise. Therefore, the underwater acoustic noise model $e(i)$ is defined as:

$$e(i) = e_{\mathrm{Gauss}}(i) + e_{\mathrm{S}\alpha\mathrm{S}}(i), \tag{10}$$

where the PDFs of $e_{\mathrm{Gauss}}(i)$, $e_{\mathrm{S}\alpha\mathrm{S}}(i)$, and σ_e and γ are provided in Eqs. (2), (8), (3) and (9), respectively.

III. Underwater Acoustic Signal Denoising Algorithm AWMF+GDES

To effectively reduce the impact of Gaussian and non-Gaussian impulsive noises on the received signal, a new underwater acoustic signal denoising method is proposed by combining the AWMF with the wavelet threshold optimization method based on GDES-ABC. The overall process of the processed scheme is shown in Fig. 2 and the specific steps are as follows.

$y(i-n)$	·····	$y(i-1)$	$y(i)$	$y(i+1)$	·····	$y(i+n)$

Fig. 3. Initial sliding window W when $L_W = 2n+1$.

A. Adaptive Window Median Filter

The SMF replaces all the samples, resulting in the distortion of the SOI. Therefore, the AWMF is proposed in this paper. First, the number of impulsive noise points in the preset window is detected, and the position of impulsive noise is determined based on the differential method, and the number of impulsive noise points is counted. Then, according to the number of impulsive noise points in the preset window, the size of the new sliding window is re-determined based on the adaptive adjustment rule. Finally, the impulsive noise points are replaced with the median point in the new window.

1) Impulsive Noise Detection: Assuming that the signal received by the receiver is $\boldsymbol{y} = [y(1), y(2), \ldots, y(N)]$, the length of the initial sliding window W is $L_W = 2n+1$ as shown in Fig. 3.

By using the initial sliding window W, the sample $w(i)$ at the i moment is obtained from the received signal $\boldsymbol{y}$ excluding the center point $y(i)$ as:

$$\begin{aligned} w(i) &= [w_1(i), w_2(i), \ldots, w_{2n}(i)] \\ &= [y(i-n), \ldots, y(i-1), y(i+1), \ldots, y(i+n)]. \end{aligned} \tag{11}$$

Sorting the signal points in $w(i)$ in ascending order to obtain:

$$\begin{aligned} r(i) &= \mathrm{sort}(w(i)) \\ &= [r_1(i), r_2(i), \ldots r_{2n}(i)], \end{aligned} \tag{12}$$

where $\mathrm{sort}(\cdot)$ is the sort function. Set $Med = \mathrm{median(r(i))}$, where $\mathrm{median}(\cdot)$ represents the median. Then, the differential noise point detector is defined as:

$$d(i) = \begin{cases} r_n(i) - y(i), & y(i) \le Med \\ r_{n+1}(i) - y(i), & y(i) > Med \end{cases}. \tag{13}$$

For a given pre-set impulsive threshold T_{noise}, if $d(i) > T_{noise}$, then $y(i)$ is an impulsive noise and $N(i) = 1$; else $y(i)$

is the no-noise SOI, and $N(i) = 0$, where $N(i)$ is the impulsive noise marker variable. In the underwater acoustic receiving signal, if the sound velocity is c, the amplitude is A, the sampling frequency is f_s, and the carrier frequency is f_c. Then, the change rate of any adjacent samples is:

$$\Delta \leq \frac{2\,A \times f_s \times \sin\left(\pi - \frac{\pi f_s}{f_c}\right)}{c}, \tag{14}$$

and the length between the adjacent samples of the underwater acoustic signal is $L_{simple} = \frac{c}{f_s}$. Therefore, the impulsive threshold is set to

$$T_{noise} = L_{simple} \times \Delta = 2A \times \sin\left(\pi - \frac{\pi f_s}{f_c}\right). \tag{15}$$

2) Adaptive Window Size Determination: The performance of the common median filters is limited by the proportion of impulsive noise in the window. The filtering performance declines with the increase in the proportion of impulsive noise. According to this proportion, this paper adaptively adjusts the size of the new window to reduce the proportion of impulsive noise and effectively improve the denoising performance.

For the initial sliding window W, the length $L_W = 2n + 1$. When the center point $y(i)$ is impulsive noise, the number of noise points in the window is calculated as:

$$Num(y(i)) = \sum_{k=-n}^{k=n} N(i+k). \tag{16}$$

Then, the length of the new window W_{new} is defined as:

$$L_{W_{new}}(y(i)) = \begin{cases} 2n+1, & 0 \leq Num(y(i)) < 4 \\ 4n+1, & 4 \leq Num(y(i)) < 8 \\ \vdots & \vdots \\ (n+1)n+1, & 2n-2 \leq Num(y(i)) < 2n+2 \end{cases}. \tag{17}$$

3) Signal Filtering: According to the size of new window $L_{W_{new}}(y(i))$ and the impulsive marker $N(i)$, the received signal is filtered as follow. The impulsive noise is replaced by the median in the new window, while the non-noise SOI remains unchanged. Suppose $y_{ip}(i)$ is an impulsive noise in W_{new}, then the other samples are:

$$\begin{aligned} w_{new}(i) &= [w_1(i), w_2(i), \ldots, w_{(L_{W_{new}}-1)/2}(i)] \\ &= [y(i - (L_{W_{new}} - 1)/2), \ldots, y(i-1), \\ &\quad y(i+1), \ldots, y(i + (L_{W_{new}} - 1)/2)]. \end{aligned} \tag{18}$$

Sorting the signal points in $w_{new}(i)$ in ascending order to obtain:

$$\begin{aligned} r_{new}(i) &= \mathrm{sort}(w_{new}(i)) \\ &= [r_1(i), r_2(i), \ldots r_{L_{W_{new}}}(i)]. \end{aligned} \tag{19}$$

Then, the impulsive noise $y_{ip}(i)$ is replaced as:

$$y'_{ip}(i) = \mathrm{median}(r_{new}(i)), \tag{20}$$

where $y'_{ip}(i)$ is the filtered signal.

B. Wavelet Threshold Optimization Based on GDES-ABC

The steps involved in the proposed wavelet threshold method are as follow. First, the appropriate wavelet basis function and the number of decomposition layers are selected to decompose the filtered signal $y'_{ip}(i)$, and the wavelet coefficients are obtained. Then an appropriate threshold and the threshold function are selected to shrink the wavelet coefficients. Finally, the estimated signal $s'(i)$ is reconstructed by inverse wavelet transform of the processed wavelet coefficients.

To overcome the limitations of traditional wavelet threshold method, this paper constructs a new threshold function and optimizes the threshold parameters using the enhanced ABC algorithm to improve the denoising performance.

1) Construction of a New Threshold Function: The threshold function reflects the different processing strategies and the estimation methods of wavelet coefficients, which directly affect the final denoising effect. The common threshold function includes hard and soft threshold functions. However, the hard threshold function is discontinuous at the threshold, leading to serious oscillation of the signal after reconstruction. While the soft threshold function shrinks the large wavelet coefficients and losses some information, leading to a deviation between the reconstructed and the SOI. Therefore, many semi-soft threshold functions have been proposed to determine a compromise strategy between hard and soft threshold functions to avoid the above-mentioned problems. Eq. (21) shows one of the semi-soft threshold function:

$$\widehat{w}_{j,k} = \begin{cases} \mathrm{sgn}\left(w_{j,k}\right)\left(|w_{j,k}| - \partial * \lambda\right), & |w_{j,k}| \geq \lambda \\ 0, & |w_{j,k}| < \lambda \end{cases}, \tag{21}$$

where $w_{j,k}$ and $\widehat{w}_{j,k}$ denote the original and the processed wavelet coefficients, respectively; λ is the threshold, and j and k denote the k^{th} coefficient of j^{th} layer; $\mathrm{sgn}(\cdot)$ is Signum function and ∂ is the regulatory factor with $0 \leq \partial \leq 1$. Eq. (21) denotes hard and soft threshold functions when $\partial = 0$ and $\partial = 1$, respectively. However, ∂ is usually set to a certain value, resulting in the lack of adaptability, and still some fixed deviations and discontinuities in the denoising process.

A reasonable threshold function needs to satisfy the continuity of the input-output curve, the processing should relatively be smooth, and the wavelet coefficient processing of the desired signal should remain unchanged. Therefore, a new adaptive threshold function is proposed in this paper as:

$$\widehat{w}_{j,k} = \begin{cases} \mathrm{sgn}\left(w_{j,k}\right)\left(|w_{j,k}| - |w_{j,k}|^{\eta(\lambda_j - |w_{j,k}|)} * \lambda_j\right), & |w_{j,k}| \geq \lambda_j \\ 0, & |w_{j,k}| < \lambda_j \end{cases}, \tag{22}$$

where η is the exponential factor having non-negative value; and λ_j denotes the j^{th} layer threshold, $j = 1, 2, \ldots, L$, where L is the number of decomposition layers.

According to the definition of continuity, it is easy to prove that Eq. (22) is continuous in the ranges of $(-\infty, -\lambda_j)$, $(-\lambda_j, +\lambda_j)$,

and $(+\lambda_j, +\infty)$. When $w_{j,k} \geq \lambda_j$, Eq. (22) can be written as:

$$\widehat{w}_{j,k} = w_{j,k} - {w_{j,k}}^{\eta(\lambda_j - w_{j,k})} * \lambda_j. \tag{23}$$

Therefore,

$$\begin{aligned}\lim_{w_{j,k}\to{\lambda_j}^+} \widehat{w}_{j,k} &= \lim_{w_{j,k}\to{\lambda_j}^+} w_{j,k} - {w_{j,k}}^{\eta(\lambda_j - w_{j,k})} * \lambda_j \\ &= \lambda_j - {\lambda_j}^{\eta(\lambda_j - \lambda_j)} * \lambda_j = 0.\end{aligned} \tag{24}$$

When $w_{j,k} = \lambda_j$, $\widehat{w}_{j,k} = 0$. And when $|w_{j,k}| < \lambda_j$, Eq. (22) can be presented as $\widehat{w}_{j,k} = 0$, then

$$\lim_{w_{j,k}\to{\lambda_j}^-} \widehat{w}_{j,k} = 0. \tag{25}$$

Thus,

$$\lim_{w_{j,k}\to{\lambda_j}^+} \widehat{w}_{j,k} = \lim_{w_{j,k}\to{\lambda_j}^-} \widehat{w}_{j,k} = 0. \tag{26}$$

It can be observed that Eq. (22) is continuous at $w_{j,k} = \lambda_j$. When $w_{j,k} < -\lambda_j$, Eq. (22) can be written as:

$$\widehat{w}_{j,k} = -\left(-w_{j,k} - (-w_{j,k})^{\eta(\lambda_j + w_{j,k})} * \lambda_j\right). \tag{27}$$

Therefore,

$$\begin{aligned}&\lim_{w_{j,k}\to(-\lambda_j)^-} \widehat{w}_{j,k} \\ &= \lim_{w_{j,k}\to(-\lambda_j)^-} -\left(-w_{j,k} - (-w_{j,k})^{\eta(\lambda_j + w_{j,k})} * \lambda_j\right) \\ &= -\left(\lambda_j - {\lambda_j}^{\eta(\lambda_j - \lambda_j)} * \lambda_j\right) = 0.\end{aligned} \tag{28}$$

When $|w_{j,k}| \leq \lambda_j$, $\widehat{w}_{j,k} = 0$, that is, $\lim_{w_{j,k}\to(-\lambda_j)^+} \widehat{w}_{j,k} = 0$. Thus,

$$\lim_{w_{j,k}\to(-\lambda_j)^-} \widehat{w}_{j,k} = \lim_{w_{j,k}\to(-\lambda_j)^+} \widehat{w}_{j,k} = 0. \tag{29}$$

And Eq. (22) is continuous at $w_{j,k} = -\lambda_j$.

When $w_{j,k} \to +\infty$,

$$\begin{aligned}\lim_{w_{j,k}\to+\infty} \frac{\widehat{w}_{j,k}}{w_{j,k}} &= \lim_{w_{j,k}\to+\infty} \frac{w_{j,k} - {w_{j,k}}^{\eta(\lambda_j - w_{j,k})} * \lambda_j}{w_{j,k}} \\ &= 1 - \lambda_j * \lim_{w_{j,k}\to+\infty} {w_{j,k}}^{\eta(\lambda_j - w_j) - 1} \\ &= 1 - \lambda_j * e^{\lim_{w_j\to+\infty}(\eta(\lambda_j - w_{j,k}) - 1)\ln w_{j,k}} \\ &= 1 - 0 = 1.\end{aligned} \tag{30}$$

When $w_{j,k} \to -\infty$,

$$\begin{aligned}\lim_{w_{j,k}\to+\infty} \frac{\widehat{w}_{j,k}}{w_{j,k}} &= \lim_{w_{j,k}\to+\infty} \frac{w_{j,k} - {w_{j,k}}^{\eta(\lambda_j - w_{j,k})} * \lambda_j}{w_{j,k}} \\ &= 1 - \lambda_j * \lim_{w_{j,k}\to+\infty} {w_{j,k}}^{\eta(\lambda_j - w_{j,k}) - 1} \\ &= 1 - \lambda_j * e^{\lim_{w_{j,k}\to+\infty}(\eta(\lambda_j - w_{j,k}) - 1)\ln w_{j,k}} \\ &= 1 - 0 = 1.\end{aligned} \tag{31}$$

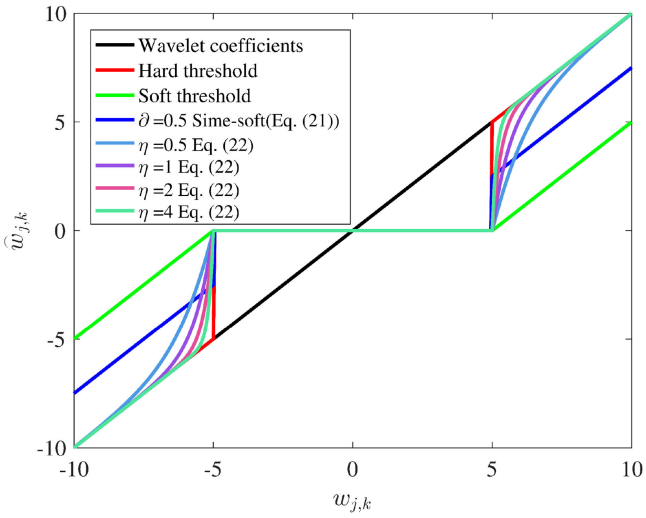

Fig. 4. Different threshold functions, when threshold $\lambda = 5$.

Thus,

$$\lim_{w_{j,k}\to\infty} \widehat{w}_{j,k} - w_{j,k} = 0. \tag{32}$$

Therefore, $\widehat{w}_{j,k} = w_{j,k}$ is an asymptote of Eq. (22).

Fig. 4 compares the different threshold functions, when threshold $\lambda = 5$. The horizontal and longitudinal axes represent the original and the processed wavelet coefficients (ranging from -10 to 10) obtained by threshold shrinkage, respectively. It can be seen from the figure that the threshold function presented in Eq. (22) is a compromise strategy between hard and soft threshold functions. It has better continuity and smoothness, while retaining larger wavelet coefficients. This means that the threshold function of Eq. (22) is more fidelity to the SOI.

2) Threshold Parameters Optimization Based on GDES-ABC: The traditional threshold estimation method based on unified threshold depends on the estimation accuracy of noise variance. When the threshold is set too small, the denoised signal still contains noise. Otherwise, it will filter out the characteristics of the SOI, resulting in the distortion of the reconstructed signal. To improve the estimation accuracy of the threshold, λ_j and η in Eq. (22) are regarded as unknown threshold parameters and are optimized using the GDES-ABC algorithm to ensure the denoising performance of the proposed algorithm.

a) Artificial bee colony algorithm: The ABC algorithm is inspired by the honey-gathering behavior of bees in nature. It abstracts the honey source into a point in the solution space, and uses the amount of honey source as the fitness value of the optimization problem. Therefore, the process of gathering honey by bees is the process of searching for the optimal solution in the solution space. The ABC algorithm mainly includes employed, onlooker and scout bees. Thus, the algorithm mainly includes four stages: initialization, employed bees, onlooker bees and scout bees.

–Initialization stage: Suppose the solution space of the optimization problem is D dimensional and the population size is

SN. The population is denoted as:

$$X_i = [x_{i1}, x_{i2}, \ldots, x_{iD}], i = 1, 2, \ldots, SN. \tag{33}$$

The upper and the lower bounds of the solution are:

$$Ub = [Ub_1, Ub_2, \ldots, Ub_D] \tag{34}$$

and

$$Lb = [Lb_1, Lb_2, \ldots Lb_D]. \tag{35}$$

The initial solution of ABC algorithm is generated randomly, and is expressed as:

$$x_{id} = Lb_d + (Ub_d - Lb_d) * rand, \tag{36}$$

where $i = 1, 2, \ldots, SN$, $d = 1, 2, \ldots, D$, $rand$ is a random real number between 0 and 1, and x_{id} denotes the d^{th} component of solution X_i.

–Employed bees stage: Each employed bee looks for only one honey source, and the process of finding the honey source is random. The new honey source is based on the current honey source field search:

$$v_{id} = x_{id} + \phi_{id}(x_{id} - x_{kd}), \tag{37}$$

where v_{id} denotes the d^{th} dimension of solution V_i, ϕ_{id} is a random real number between -1 and 1, and x_{kd} denotes a randomly selected neighbor of x_{id}, $k \in \{1, 2, \ldots, SN\}$, $k \neq i$.

After the new solution is generated, the population is updated using the greedy selection strategy according to the fitness value. The fitness value fit_i of solution X_i is calculated by:

$$fit_i = \begin{cases} \frac{1}{1+f_i} & f_i \geq 0 \\ 1 + |f_i| & \text{otherwise} \end{cases}, \tag{38}$$

where f_i is the objective function value by bringing solution X_i into the optimization problem.

According to the greedy selection strategy, if the fitness value of the new solution V_i is larger than that of the current solution X_i, then V_i is a better solution that replaces X_i, and the population is updated. Otherwise, V_i is a worse solution, and is abandoned, keeping the population unchanged while the repeated value $trial(i)$ adds 1, where $trial(i)$ denotes the number of repeated searches for bee i.

–Onlooker bees stage: The searching process of onlooker bees is based on the honey source obtained by employed bees. The onlooker bees generate new solutions using Eq. (37) according to the selection probability $p_{accept}(i)$. Then the population is updated using the greedy selection strategy. The selection probability $p_{accept}(i)$ is calculated by:

$$p_{accept}(i) = \frac{fit_i}{\sum_{j=1}^{SN} fit_j}. \tag{39}$$

–Scout bees stage: When a solution is not improved within the previously set number of searches (denoted as $limit$), this solution is abandoned. Then, a new solution is randomly generated using Eq. (36) to replace the abandoned solution.

Although, the ABC algorithm has good convergence performance, the random generation of the initial population leads to the lack of diversity of the population, and the convergence speed of the random neighborhood search method is slow. Moreover, the update method based on greedy selection strategy directly abandons the bad solutions, which significantly reduces the development ability of the colony and makes the algorithm to fall into local optimum that can result in poor convergence accuracy and even non-convergence.

Algorithm 1: GDES-ABC Algorithm.

Initialization: Generate the initial population using Eqs. (40)-(42); set SN, D, Ub, Lb, T_0, K, $p_{\max}$, $p_{\min}$, $limit$, $t_{\max}$; and $t = 1$;
while $t <= t_{\max}$ **do**
  Calculate the center of a dynamic elite group with Eq. (45);
  for $i = 1 : SN$ **do**
    Randomly select a solution X_t from the population;
    Generate a new solution V_t with Eq. (44);
    Evaluate the fitness value fit_v of V_t, and fit_x of X_t;
    if $fit_v > fit_x$ **then**
      $X_t = V_t$, $fit_x > fit_v$, $trial(t) = 0$;
    else if $e^{-[fit_v - fit_x]/KT_t} < rand$ **then**
      $X_t = V_t$, $fit_x > fit_v$, $trial(t) = trial(t) + 1$;
    else
      $trial(t) = trial(t) + 1$;
    end if
  end for
  Update the center of the dynamic elite group with Eq. (45);
  $flag = 1$;
  for $i = 1 : SN$ **do**
    if $flag = 1$ **then**
      Randomly select a solution X_t from the dynamic elite group;
    end if
    Generate a new solution V_t with Eq. (44);
    Evaluate the fitness value fit_v of V_t, and fit_x of X_t;
    if $fit_v > fit_x$ **then**
      $X_t = V_t$, $fit_x > fit_v$, $trial(t) = 0$, $flag = 0$;
    else if $e^{-[fit_v - fit_x]/KT_t} < rand$ **then**
      $X_t = V_t$, $fit_x > fit_v$, $trial(t) = trial(t) + 1$, $flag = 1$;
    else
      $trial(t) = trial(t) + 1$, $flag = 1$;
    end if
  end for
  Record the current optimal solution X_{Gbest};
  if $trial(t) > limit$ **then**
    Replace X_t by a new solution generated by Eq. (36);
    $trial(t) = 0$;
  end if
  $t = t + 1$; $T_t = T_{t-1} * e^{-0.7T_{t-1}/\sigma_{fit}}$;
end while
Output: The global optimal solution X_{opt}.

b) GDES algorithm: To overcome the shortcomings of the ABC algorithm and obtain the optimal threshold parameters in Eq. (22), the GDES-ABC algorithm is proposed in this paper based on three improvement strategies. The pseudocode of the proposed GDES-ABC algorithm is provided in Algorithm 1, and the main improvements are summarized as follows.

–Population initialization based on good point set: The first improvement strategy of the proposed GDES-ABC algorithm is to initialize the population based on good point set. The population initialization based on good point set can effectively improve the diversity of the population and prevent the algorithm from falling into a local optimum. The method of constructing

good points is:

$$r_k = \mathrm{deci}\left\{2\cos\frac{2\pi k}{p}\right\}, 1 \le k \le D, \tag{40}$$

where p denotes the minimum prime number, and $(p-3)/2 \ge D$; D is the dimension of the solution; $\mathrm{deci}\{\cdot\}$ denotes obtaining the decimal, and r_k denotes the good points. Therefore, the construction method of good point set $[P_{SN}(1), P_{SN}(2), \ldots, P_{SN}(SN)]^T$ is given by:

$$P_{SN}(i) = \{\mathrm{deci}\{r_1 * i\}, \ldots, \mathrm{deci}\{r_D * i\}\}, i = 1, \ldots, SN, \tag{41}$$

where $[\cdot]^T$ denotes the transpose and SN is the the population size. Then, the initial population is obtained by:

$$X_i = Lb + (Ub - Lb) * P_{SN}(i), i = 1, \ldots, SN, \tag{42}$$

where Ub and Lb are the upper and the lower bounds of the solution, respectively.

–Neighborhood searching based on dynamic elite group: The second improvement strategy of the proposed GDES-ABC algorithm is to perform neighborhood search based on the dynamic elite group. The dynamic elite group contains better solutions in the population, and its size varies with the number of iterations. Therefore, the neighborhood searching based on dynamic elite group can effectively accelerate the convergence speed and improve the searching efficiency. According to the fitness value, the dynamic elite group $\mathbf{DXE} = [DXE_1, DXE_2, \ldots, DXE_{Telite}]^T$ is constructed by the top $Telite = \mathrm{ceil}(p_{Elite} * SN)$ honey bees, where $\mathrm{ceil}(\cdot)$ denotes rounding up and p_{Elite} is the proportion of dynamic elite group in the population, which is given by:

$$p_{Elite} = p_{\max} + \left(\frac{t_{\max} - t}{t_{\max}}\right) * (p_{\min} - p_{\max}), \tag{43}$$

where $p_{\max}$ and $p_{\min}$ are the maximum and the minimum values of p_{Elite}, respectively; $t_{\max}$ is the maximum number of iterations and t is the current iteration number. It can be seen from Eq. (43) that, in the early stage of the algorithm, both t and p_{Elite} are small, and this elite group contains the best few solutions. Therefore, the neighborhood searching method based on this elite group is more decisive and the convergence speed can be significantly accelerated. However, in the later stage of the algorithm, both t and p_{Elite} are large, and this elite population contains a large number of solutions from which some might be poor solutions. Therefore, the population is more diverse, and the ability to prevent falling into the local optimum and find the global optimum is strengthened.

The improved neighborhood searching method based on the dynamic elite group of GDES-ABC algorithm is given by:

$$v_{id} = DXEC_d + \phi_{id}(Gbest_d - x_{kd}), d = 1, 2, \ldots, D, \tag{44}$$

where ϕ_{id} is a random real number between -1 and 1, $Gbest$ is the global optimum, x_{kd} is a randomly selected neighbor of x_{id}, and $DXEC = [DXEC(1), DXEC(2), \ldots, DXEC(D)]$ is a center of the elite group, which is given by:

$$DXEC(d) = \frac{1}{Telite}\sum_{n=1}^{Telite}\mathbf{DXE}_{nd}, d = 1, 2, \ldots, D. \tag{45}$$

The neighborhood searching strategy based on the dynamic elite group can be described as follows. For each neighborhood search, the employed bees randomly search the neighborhood with the same probability, and a new solution is generated using Eq. (44). The onlooker bees search the neighbor randomly to form the dynamic elite group and generate a new solution using Eq. (44). For onlooker bees, if the new solution is better than the previous one, it is selected for the next neighborhood search; otherwise, a new onlooker bee in the dynamic elite group is randomly selected in the next neighborhood search. This neighborhood searching strategy is carried out in a random manner to ensure the population diversity and avoid the invalid search.

–Simulated annealing selection mechanism: The third improvement strategy of the proposed GDES-ABC algorithm is simulated annealing selection mechanism. According to a certain probability, the simulated annealing selection mechanism accepts poor solutions that can effectively prevent the algorithm from falling into a local optimum and enhance the ability of the algorithm to search for the global optimum. Assume that the current temperature is T_t at the t^{th} iteration and the annealing parameter is K, then a new solution V_t is generated using Eq. (43) with fitness value fit_v. The simulated annealing selection mechanism is as follows: If $fit_v > fit_x$, the new solution is accepted directly, where fit_x is the fitness value of the current solution; otherwise, the new solution is accepted according to the acceptance probability p'_{accept} that changes with the number of iterations. The acceptance probability is calculated as:

$$p'_{accept} = e^{-[fit_v - fit_x]/KT_t} < rand, \tag{46}$$

where

$$T_t = T_{t-1} * e^{-\varsigma T_{t-1}/\sigma_{fit}}, \tag{47}$$

where ς is a constant and $\varsigma \le 1$, which is usually set to 0.7, and σ_{fit} is the standard deviation of fitness value of all solutions.

It can be seen from Eqs. (46)-(47) that, t is small and T_t is high in the early stage of the algorithm. Hence, p'_{accept} is high, which implies that the algorithm accepts some poor solutions, and the bee colony has strong development ability. However, in the later stage of the algorithm, t becomes large, and T_t gradually decreases. Hence, p'_{accept} becomes smaller. Therefore, the algorithm rejects the poor solutions, ensures the ability of the algorithm to search for the optimal solution, and avoids invalid search.

c) The fitness function: The MSE between the SOI and the reconstructed signal can be used as the fitness function [33], [34], [40]. Therefore, the optimal threshold parameter in Eq. (22) is obtained by minimizing the MSE between the training and the reconstructed signals using the GDES-ABC algorithm. The fitness function is defined as:

$$fit = \mathrm{MSE}(s, s') = \frac{1}{N}\sum_{i=1}^{N}|s(i) - s'(i)|^2, \tag{48}$$

where $s(i)$ and $s'(i)$ are the training and the reconstructed signals, respectively, and N is the length of the signal. It can be seen that the threshold function shown in Eq. (22) is a function of the threshold parameters λ_j and η. Once both λ_j and η

TABLE I
BENCHMARK FUNCTIONS

Names	Functions	Ranges	Optimal value	Accepted values
Sphere	$f_1(x) = \sum_{i=1}^{D} x_i^2$	$[-100, 100]^D$	0	1×10^{-8}
Step	$f_2(x) = \sum_{i=1}^{D} (\lfloor x_i + 0.5 \rfloor)^2$	$[-100, 100]^D$	0	1×10^{-8}
Rastrigin	$f_3(x) = \sum_{i=1}^{D} [x_i^2 - 10\cos(2\pi x_i) + 10]$	$[-5.12, 5, 12]^D$	0	1×10^{-8}
Ackley	$f_4(x) = 20 + e - 20\exp\left(-0.2\sqrt{\frac{1}{D}\sum_{i=1}^{D} x_i^2}\right) - \exp\left(\frac{1}{D}\sum_{i=1}^{D}\cos(2\pi x_i)\right)$	$[-50, 50]^D$	0	1×10^{-8}
Schwefel 2.26	$f_5(x) = 418.9828 \times D - \sum_{i=1}^{D} x_i \sin\left(\sqrt{\lvert x_i \rvert}\right)$	$[-500, 500]^D$	0	1×10^{-8}
RosenBrock	$f_6(x) = \sum_{i=1}^{D-1} \left[100(x_{i+1} - x_i^2) + (x_i - 1)^2\right]$	$[-5, 10]^D$	0	1×10^{-1}

are determined, Eq. (22) is also determined. Then, the wavelet coefficients can be obtained after threshold shrinkage and the denoising signal $s'(i)$ can be reconstructed. Therefore, in the GDES-ABC algorithm, the vector composed of λ_j and η can be regarded as the location of the honey source, and the optimal threshold parameters can be obtained by minimizing the fitness function shown in Eq. (48).

IV. NUMERICAL SIMULATION

In the numerical simulation, the efficiency of the proposed GDES-ABC algorithm, the wavelet threshold optimization method based on GDES-ABC, and the underwater acoustic signal denoising algorithm based on AWMF+GDES are verified.

A. Simulated Results of GDES-ABC

To verify and compare the performance of the GDES-ABC algorithm with ABC, ECABC, PSO, and MPSO algorithms, six benchmark functions were selected. Table I shows the six benchmark functions, where f_1 and f_2 are the continuous unimodal function and the discontinuous step function, respectively; $f_3 - f_5$ are the continuous multimodal functions. When $D \leq 3$, f_6 is a unimodal function and when D > 3, f_6 turns into a multimodal function. For $f_1 - f_5$, the optimal value is 0, while the acceptable value is 1×10^{-8} that represents the satisfactory solution of the function, and for f_6, the optimal value is 0 too while the acceptable value is 1×10^{-1}. D is the dimension of the solution. The simulations were performed using MATLAB R2015b running on a computer with Intel i5-4570 processor and 4G memory.

Fig. 5 shows the convergence performances of different algorithms on $f_1 - f_6$. The parameter settings of GDES-ABC used in simulations are shown in Table II, where the other parameters of PSO, MPSO, ABC and ECABC algorithms are shown in Table III. It can be seen from Fig. 5 that ABC, ECABC, GDES-ABC, and MPSO algorithms obtain satisfactory solutions for f_1 where the convergence speed of the GDES-ABC algorithm is at least 25% higher than the other algorithms. In addition, when the iteration number $t = 1000$, the convergence precision of GDES-ABC is at least 21% higher than the other algorithms.

TABLE II
PARAMETER SETTINGS OF GDES-ABC

Parameter	Value
Size of population	50
Dimension of the solution	20
Initial temperature	3000°C
Annealing parameter	0.98
Maximum proportions of the dynamic elite group	0.8
Minimum proportions of the dynamic elite group	0.2
Maximum number of repeated searches	100
Maximum number of iterations	1000

TABLE III
PARAMETER SETTINGS OF PSO, MPSO, ABC AND ECABC

Parameter	Value
Size of population	50
Dimension of the solution	20
Proportions of the elite group of ECABC	0.4
Self-recognition component of PSO	2
Social component of PSO	2
Inertia weight of PSO	0.8
Maximum value of inertia weight of MPSO	0.9
Minimum value of inertia weight of MPSO	0.4
Maximum values of Social component and Self-recognition component of MPSO	2.5
Minimum values of Social component and Self-recognition component of MPSO	0.5
Decreasing rate of the inertia weight of MPSO	10
Mutation probability of MPSO	0.4

For f_2, ABC, ECABC, GDES-ABC, and MPSO algorithms obtain the global optimum where PSO algorithm falls into a local optimum, and the convergence speed of GDES-ABC is at least 33% higher than the other algorithms. For f_3, the GDES-ABC algorithm obtains the global optimum at $t = 300$ while both PSO and MPSO fall into local optimum, and the convergence speed of GDES-ABC is at least 20% higher than the other algorithms. For f_4, only the GDES-ABC and the ECABC algorithms obtain satisfactory solutions, and the convergence speed of GDES-ABC

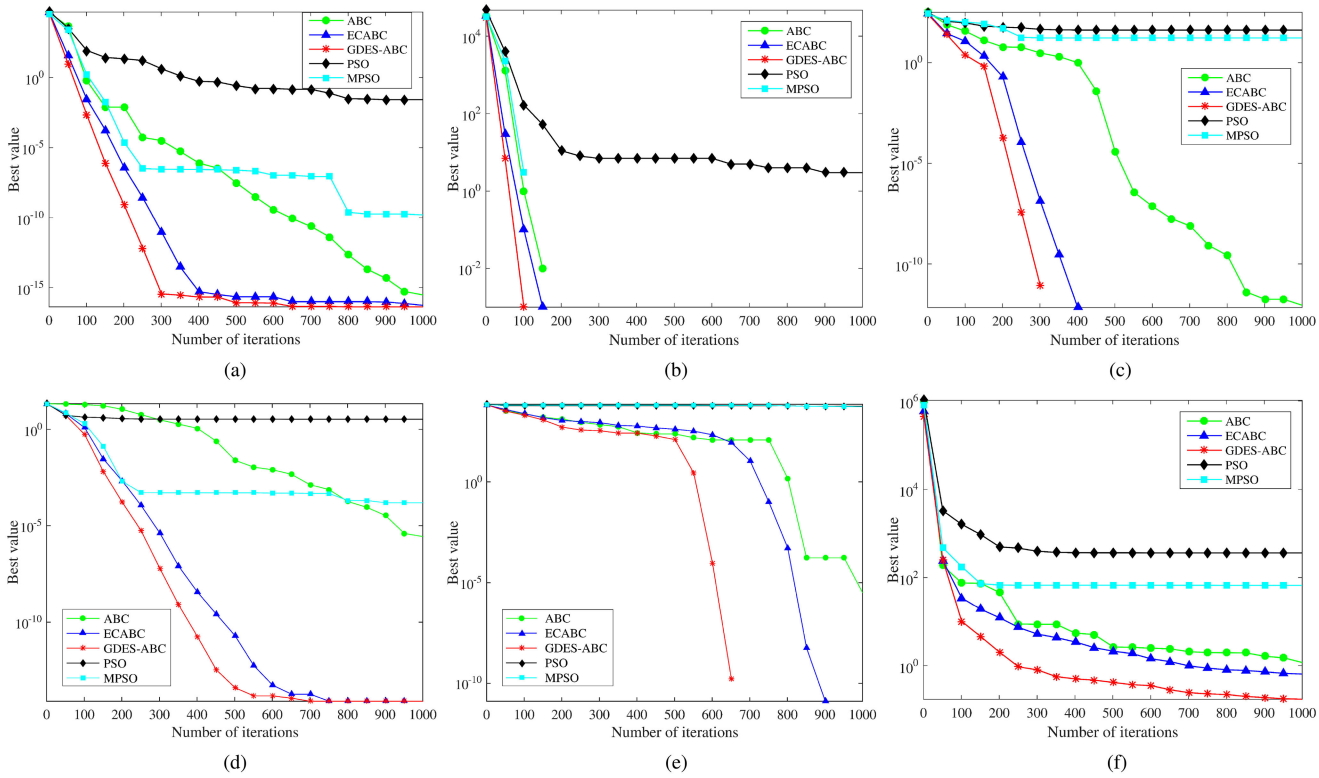

Fig. 5. Convergence performances of different algorithms on six different benchmark functions, $f_1 - f_6$. (a) f_1. (b) f_2. (c) f_3. (d) f_4. (e) f_5. (f) f_6.

TABLE IV
COMPLEXITIES AND AVERAGE RUNNING TIMES OF ABC, ECABC, AND GDES-ABC ALGORITHMS FOR THE 6 BENCHMARK FUNCTIONS $f_1 - f_6$

Algorithms	Complexity	Ave-time (s)					
		f_1	f_2	f_3	f_4	f_5	f_6
ABC	$O(D \cdot SN)$	2.281	3.072	3.463	3.925	3.041	3.140
ECABC	$O(D \cdot SN + SN \cdot \log(SN) + SN)$	2.792	3.371	3.716	4.169	3.550	3.285
GDES-ABC	$O(D \cdot SN + SN \cdot \log(SN) + SN + 2 \cdot D + 1)$	3.475	3.641	3.722	4.050	3.602	3.766

is at least 23% higher than the ECABC. For f_5, only the GDES-ABC obtains the global optimum. For f_6, only the GDES-ABC and the ECABC algorithms obtain satisfactory solutions, and the convergence speed of GDES-ABC is at least 66% higher than the ECABC. When $t = 1000$, the convergence precision of GDES-ABC is at least 73% higher than the ECABC. Overall, the proposed GDES-ABC algorithm achieves better performance in terms of convergence speed and convergence precision than the other algorithms.

Fig. 5 shows that the convergence performances of ABC, ECABC, and GDES-ABC algorithms are generally better than PSO and MPSO algorithms. For further comparison, Table IV only lists the computational complexities and the average running times of ABC, ECABC, and GDES-ABC algorithms for $f_1 - f_6$. Each algorithm was run for 50 times, and the average running time was calculated for each function. The ABC algorithm mainly includes population update and fitness calculation, and the computational complexity is $O(D \cdot SN)$. The ECABC algorithm has the computational complexity of $O(D \cdot SN + SN \cdot \log(SN) + SN)$, which mainly lies in selecting the elite population and computing the elite population center. The computational complexity of the proposed GDES-ABC is $O(D \cdot SN + SN \cdot \log(SN) + SN + 2 \cdot D + 1)$ and is mainly in the population initialization based on good point set, the neighborhood searching based on the dynamic elite group, and the simulated annealing selection mechanism. It can be seen form Table IV that the average running time of the GDES-ABC algorithm is slightly longer than that of the ABC algorithm. However, there is no significant difference in the average running times of GDES-ABC and ECABC algorithms. Considering the fact that the proposed GDES-ABC algorithm has higher complexity than the other two algorithms, the average running time of the proposed algorithm is acceptable.

B. Simulated Results of the Wavelet Threshold Optimization Method Based on GDES-ABC

To verify the effectiveness of the proposed wavelet threshold optimization method based on GDES-ABC in removing the

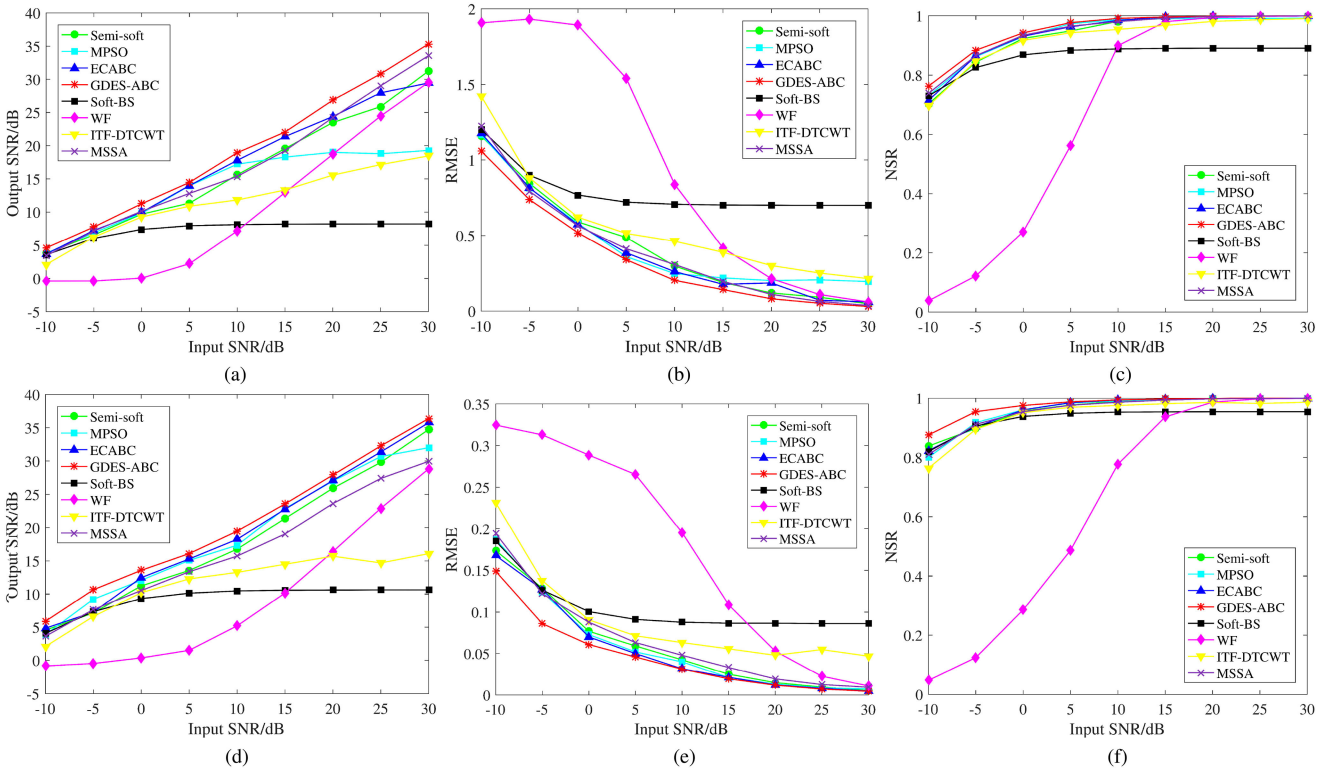

Fig. 6. Comparison of output SNRs, RMSEs, and NSRs of denoising two benchmark signals using different denoising algorithms. (a) Output SNR of Bumps. (b) RMSE of Bumps. (c) NSR of Bumps. (d) Output SNR of Doppler. (e) RMSE of Doppler. (f) NSR of Doppler.

Gaussian noise, its performance in denoising the two benchmark signals, named as Bumps and Doppler, is compared with the wavelet semi-soft threshold function with unified threshold method (Semi-soft), Bayes shrink method with soft threshold function (Soft-BS), wiener filter (WF), ITF-DTCWT, and the wavelet threshold optimization methods based on MPSO and ECABC (MPSO and ECABC). The noise is AWGN. The output SNR, RMSE, and NSR are used to evaluate the performance of denoising and are defined as:

$$\mathrm{SNR} = 10\log_{10}\frac{\sum_{i=1}^{N} s^2(i)}{\sum_{i=1}^{N}\left[s(i)-s'(i)\right]^2}, \tag{49}$$

$$\mathrm{RMSE} = \sqrt{\frac{1}{N}\sum_{i=1}^{N}\left(s(i)-s'(i)\right)^2}, \tag{50}$$

$$\mathrm{NSR} = \frac{\sum_{i=1}^{N}\left(s(i)-\bar{s}\right)\left(s'(i)-\bar{s}'\right)}{\sqrt{\sum_{i=1}^{N}\left[s(i)-\bar{s}\right]^2 \times \sum_{i=1}^{N}\left[s'(i)-\bar{s}'\right]^2}}, \tag{51}$$

where $s(i)$ and $s'(i)$ are the SOI and the reconstructed signal, respectively; $\bar{s}$ and $\bar{s}'$ are the means of $s(i)$ and $s'(i)$, respectively; and N is the length of the signal.

Fig. 6 compares the output SNRs, RMESs, and NSRs of denoising the two benchmark signals using different algorithms. The input SNR is defined as Eq. (3), ranging from -10 dB to 30 dB. Where the wavelet basis function used in this paper is sym7, and the number of decomposition layers is $L = 5$. The orders of WF is 100. The ITF-DTCWT performs a 4-level transform on the noising signal using the 13,19-tap filters for level 1 and the Q-shift 14-tap filters for level 2. The lengths of samples and training signals are $N_{snap} = 1024$, and $N_{train} = 100$, respectively, while the maximum number of iterations is 300. It can be seen from the figures that for the two different benchmark signals, the proposed GDES-ABC method yields better performance than the other algorithms in terms of output SNRs, RMSEs, and NSRs. Moreover, when the input SNR is small, the noise component is large, and it is difficult for most algorithms to extract the signal component. However, the proposed threshold function has better differentiability and continuity, and can extract the SOI from the noise environment more clearly than the other algorithms, obtaining a better denoising performance. When the input SNR continues to increase, the signal energy is enhanced, and the algorithms can clearly distinguish between noise and signal energies to obtain better denoising performance. Moreover, the performance of the wavelet threshold optimization methods is stronger than that of non-optimization algorithms. Due to the superior optimization ability of the GDES-ABC algorithm, the proposed wavelet threshold optimization method obtains the best performance. Besides, when the input SNR is small, the WF is sensitive to noise, and it is difficult to obtain satisfactory denoising performance. With the increase of the input SNR, the performance of WF has improves rapidly, even surpassing the MPSO and ITF-DECWT. However, the performance of the Soft-BS increases first with the increase in the input SNR and

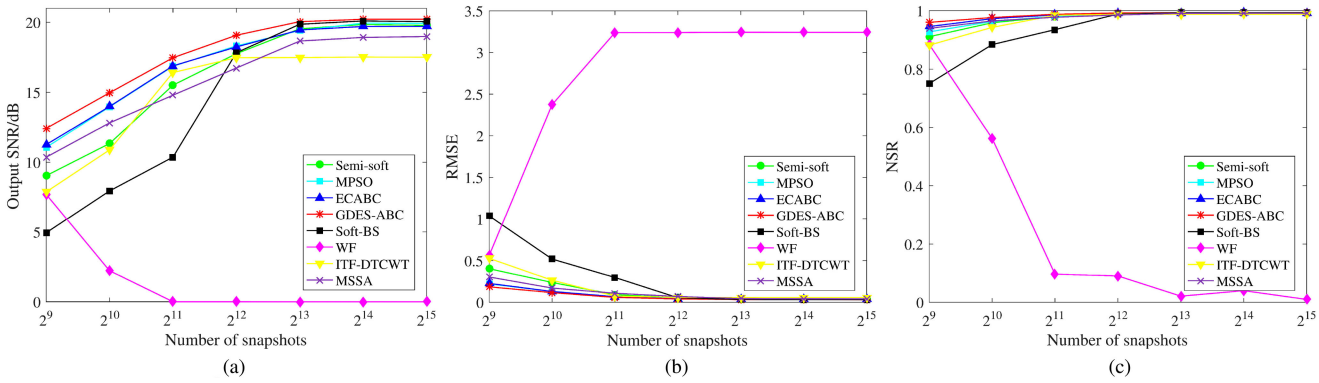

Fig. 7. Comparison of output SNRs, RMSEs, and NSRs of different denoising algorithms under different numbers of sample points. (a) Output SNR. (b) RMSE. (c) NSR.

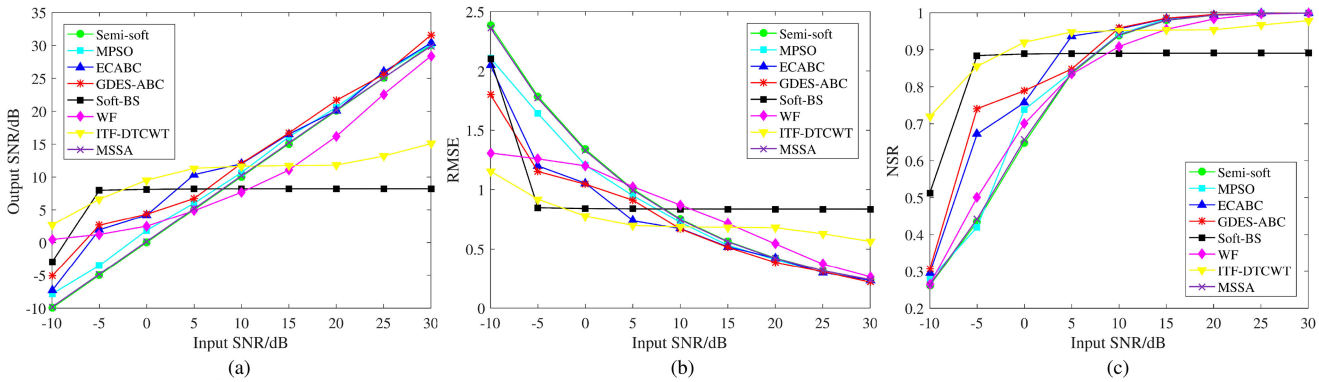

Fig. 8. Comparison of output SNRs, RMSEs, and NSRs under narrowband Gaussian noise using different denoising algorithms. (a) Output SNR. (b) RMSE. (c) NSR.

then tends to be stable. This is because Soft-BS uses a soft threshold function to process wavelet coefficients, leading to a deviation between the reconstructed and the original signals and achieving stable performance. Although the threshold function of the ITF-DECWT method has continuity and divergence, it lacks self-adaptability, resulting in poor denoising performance. Furthermore, for Bumps signal, the output SNRs of the GDES-ABC algorithm are slightly higher than the other algorithms when input SNR $\leq$ 15 dB. However, the output SNRs of the GDES-ABC algorithm increase rapidly and become significantly higher than the other algorithms for input SNR $>$ 15 dB. When the input SNR $=$ 30 dB, the output SNR of the GDES-ABC method is 4.09 dB higher than the other algorithms. Overall, the efficient optimization ability of the GDES-ABC algorithm enables the proposed algorithm to achieve the highest output SNR and NSR and the minimum RMSE compared with the other algorithms for the two benchmark signals.

Fig. 7 compares the output SNRs, RMSEs, and NSRs of the 8 algorithms with different numbers of sample points. Where the Bumps is used as the SOI, the input SNR $=$ 5 dB, $N_{train}=$ 100, and the number of sample points N_{snap} ranges from 2^9 to 2^{15}. It can be seen from Fig. 7 that the proposed algorithm obtains the highest output SNR and NSR and the minimum RMSE compared to the other algorithms.The denoising performant of most algorithms improves with the increase in N_{snap}. However, the performance of the WF gradually decreases as the number of sample points increases. The reason is that the order of the WF cannot meet the demand for a large number of sample points, and the denoising performance decreases. On the other hand, the proposed algorithm can obtain the best performance when the number of sample points is small, indicating that the proposed algorithm is more suitable for underwater sparse channel compared with other algorithms.

To test the robustness of the wavelet threshold optimization method based on GDES-ABC, Fig. 8 shows the output SNRs, RMSEs, and NSRs of different denoising algorithms with the input SNR under narrowband Gaussian noise. The parameters of each algorithm are similar to the parameters mentioned above. $N_{train} = 100$, and $N_{snap} = 1024$. It can be seen from Fig. 8 that the output SNR and NSR of the wavelet threshold optimization methods such GDES-ABC, ECABC, MPSO, are lower and the RMSEs are smaller than that of other algorithms when input SNR $>$ 10 dB. The reason is that the wavelet coefficient of the narrowband noise is relatively larger, and does not obey the Gaussian distribution when the input SNR is small. Thus, it is difficult for these methods to estimate the optimal threshold

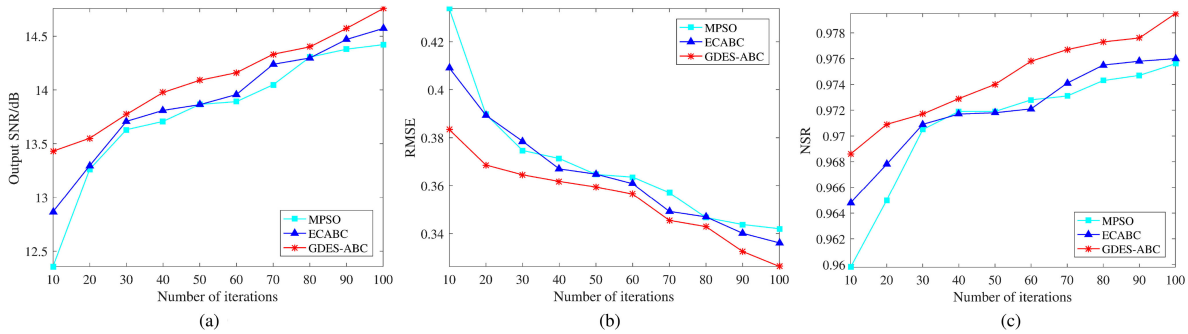

Fig. 9. Comparison of output SNRs, RMSEs, and NSRs of three different wavelet threshold optimization methods under different numbers of iterations. (a) Output SNR. (b) RMSE. (c) NSR.

parameters. Among them, Soft-BS and ITF-DTCWT can obtain better threshold by using Bayesian estimation method and the improved threshold determination method, respectively, to obtain better performance. However, when the input SNR $>$ 10 dB, the performances of the wavelet threshold optimization methods are better than that of non-optimization algorithms. The reason is that, with the increase of input SNR, the wavelet coefficient from the SOI is larger than that of the narrowband noise. In this case, these methods can obtain better threshold parameters and better performance. Although, the performance of the GDES-ABC algorithm is poor when the input SNR is small, it still achieves the best performance among the wavelet threshold optimization methods. In addition, when the input SNR is large, the GDES-ABC algorithm achieves the best performance in all algorithms, indicating that the proposed algorithm has a certain degree of adaptability to remove the narrowband noise.

Fig. 9 shows the comparison of output SNRs, RMSEs, and NSRs of three wavelet threshold optimization methods under different numbers of iterations. Where the Bumps is used as the SOI, the input SNR $=$ 5 dB, $N_{train}=$ 100, and N_{snap} $=$ 1024. It can be seen from the figure that the output SNRs and NSRs of the three methods improve with the increase in the number of iterations. Meanwhile, the proposed algorithm obtains the highest output SNR and NSR compared with the other methods. Moreover, when the number of iterations reaches 100, the performance of all three wavelet threshold optimization methods does not stabilize. It can be inferred that the performance of the three methods will be improved with the increase in numbers of iterations. These results are consistent with the convergence performance analysis of the optimization algorithm presented in section IV-A and further validate that the proposed GDES-ABC algorithm has a better performance in terms of convergence speed and convergence precision than the other algorithms.

C. Simulated Results of the Underwater Acoustic Signal Denoising Algorithm Based on AWMF+GDES

In underwater acoustic communication, QPSK and 16QAM signals are widely used. These signals are considered as the SOI in this paper, and the underwater acoustic noise is obtained by combining the AWGN with the non-Gaussian impulsive noise shown in Eqs. (2) and (8), respectively. The performance of the proposed underwater acoustic signal denoising algorithm based on AWMF+GDES is presented and compared with different algorithms obtained by combining AWMF, with Semi-soft, MSSA, MPSO, and ECABC.

TABLE V
PARAMETER SETTINGS OF AWMF+GDES

Parameter	Value
Carrier frequency of QPSK	12kHz
Carrier frequency of 16QAM	20kHz
Characteristic exponent	1.5
Local parameter	0
Symmetric parameter	0
Length of the initial sliding window	7
Length of the train signal	1024
Length of the signal	10000

Fig. 10 shows the comparison of output SNRs, RMSEs, and NSRs (when input MSNR $=$ 20 dB) after denoising QPSK and 16QAM signals using the proposed AWMF+GDES, the AWMF, the AWMF+MPSO, the AWMF+ECABC, the AWMF+Semi-soft, the AWMF+MSSA, and the SMF methods. The parameter settings of the proposed algorithm used in the simulations are shown in Tables II and V. It can be seen that for both QPSK and 16QAM signals, the output SNRs and NSRs of all the 7 algorithms increase at first with the increase in the input SNR, and then tend to saturate. While the RMSEs of all the 7 algorithms gradually decrease and tend to flatten. The reason for this is that both the non-Gaussian impulsive noise and the Gaussian noise are strong when MSNR $=$ 5 dB and input SNR is small. Therefore, the SOI is blurred by the strong underwater acoustic noise, and the performance of all denoising algorithms is poor. As the input SNR gradually increases, the power of the SOI also increases. Thus, the denoising algorithms can separate SOI more clearly, and the performance increases accordingly. It can be seen from the two curves obtained by AWMF and SMF that, the proposed AWMF obtains higher output SNR and NSR and a smaller RMSE than the SMF due to the ability to adaptively adjust the size of the median filter window. In addition, the performance of the optimized denoising algorithms is better than that of the non-optimized algorithms. This shows that the optimized denoising algorithm can effectively improve the

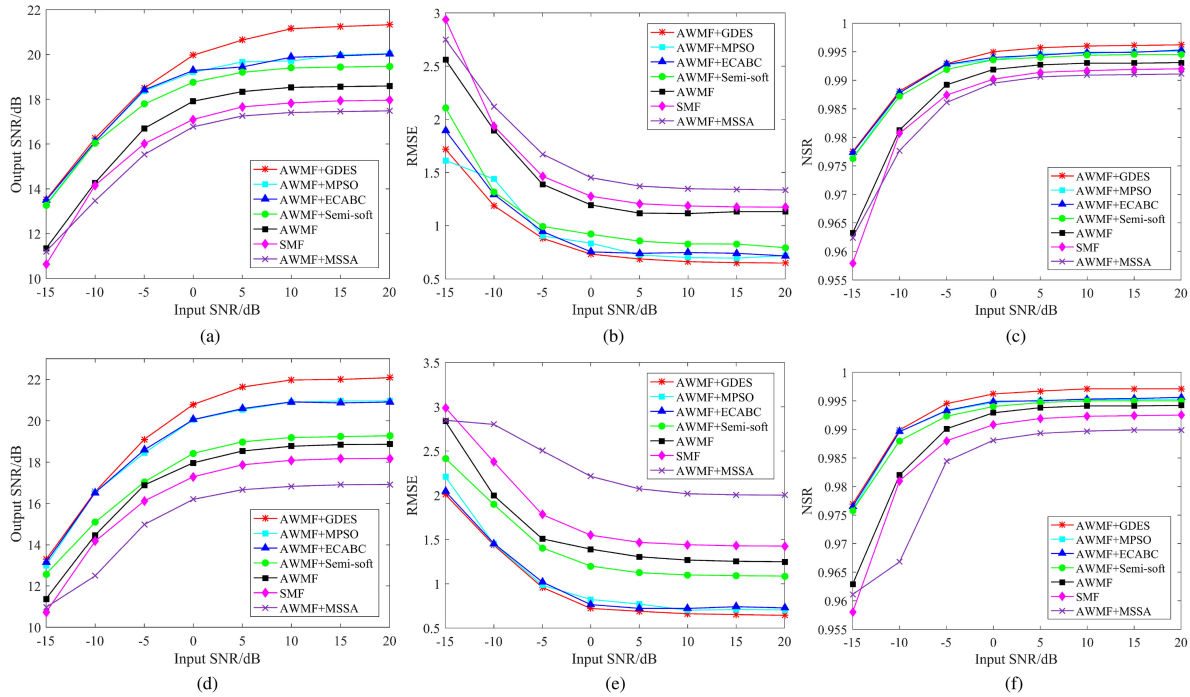

Fig. 10. Comparison of output SNRs, RMSEs and NSRs as a function of the input SNR (when input MSNR = 20 dB) after denoising QPSK and 16QAM signals using 7 different algorithms. (a) Output SNR of QPSK. (b) RMSE of QPSK. (c) NSR of QPSK. (d) Output SNR of 16QAM. (e) RMSE of 16QAM. (f) NSR of 16QAM.

denoising performance of the traditional denoising algorithm. Moreover, the proposed AWMF+GDES algorithm obtains the highest output SNRs for QPSK and 16QAM signals when the input SNR > -5 dB and SNR > -10 dB, respectively. It can be seen that the proposed AWMF+GDES algorithm is more suitable for denoising the 16QAM signal, which means it is more suitable for high-speed underwater acoustic communication.

Fig. 11 shows the comparison of output SNRs, RMSEs, and NSRs as a function of the input MSNR (when input SNR = 5 dB) using 7 different algorithms. It can be seen that for each SOI, the output SNRs, RMSEs, and NSRs of all the 7 algorithms gradually increase with the increase in the input MSNR, and the NSRs tend to saturate. However, the RMSEs of all the 7 algorithms gradually increase faster with the increase in the input MSNR. The reason is that the amplitude of the SOI is getting larger with the increase in the input MSNR and the RMSEs after denoising are also increasing. Overall, the proposed AWMF+GDES algorithm obtains the highest output SNRs and NSRs, and the minimum RMSEs than the other 6 algorithms. It means that the proposed AWMF+GDES algorithm can obtain better performance for deniosing the underwater acoustic signals.

V. Experimental Results

In this section, the performance of the proposed underwater acoustic signal denoising algorithm is evaluated with real data collected during two sea trials. The first sea trial was performed in a shallow-water acoustic channel at Qingdao landing stage, Qingdao, China, on August 24, 2020. The depth of the experiment field was about 4 m. The signals were transmitted between two transducers under the bridge. Both the transducers were suspended at a depth of 2 m. The average distance between the transducers was 60 m. The second sea trial was performed in a shallow-water acoustic channel at Jiaozhou Bay, Qingdao, China, on September 22, 2020, and the average distance between the transducers is 120 m. The depth of the experiment field was about 30 m. The two transducers were carried on two fishing boats. Both the transducers are suspended at a depth of 4 m under the boats. The modulation format during the two sea trials was BPSK with a bit rate of 3.5 k bps and a carrier frequency of 14 kHz.

The algorithm parameters of each algorithm are similar to the numerical simulation presented in Section IV. Fig. 12 shows the denoising results of the proposed AWMF+GDES algorithm for a BPSK signal at the two sea trials. It can be seen that both the original signals are blurred by the underwater acoustic noise. When the average distance between the transducers was 60 m, there was a small amount of non-Gaussian impulsive noise. And when the average distance between the transducers was 120 m, the BPSK signal was seriously blurred by the non-Gaussian impulsive noise. However, after using the proposed algorithm, most of the noise is eliminated, and the denoised signals retain detail information of the original signals.

Table VI compares the output SNRs, RMSEs and NSRs obtained by different methods during the two sea trials. When the average distance between transducers was 60 m, the SNRs, RMSEs, and NSRs obtained by each algorithm were similar. The reason is that the SOI was less affected by the underwater noise because the average distance between the transducers was short.

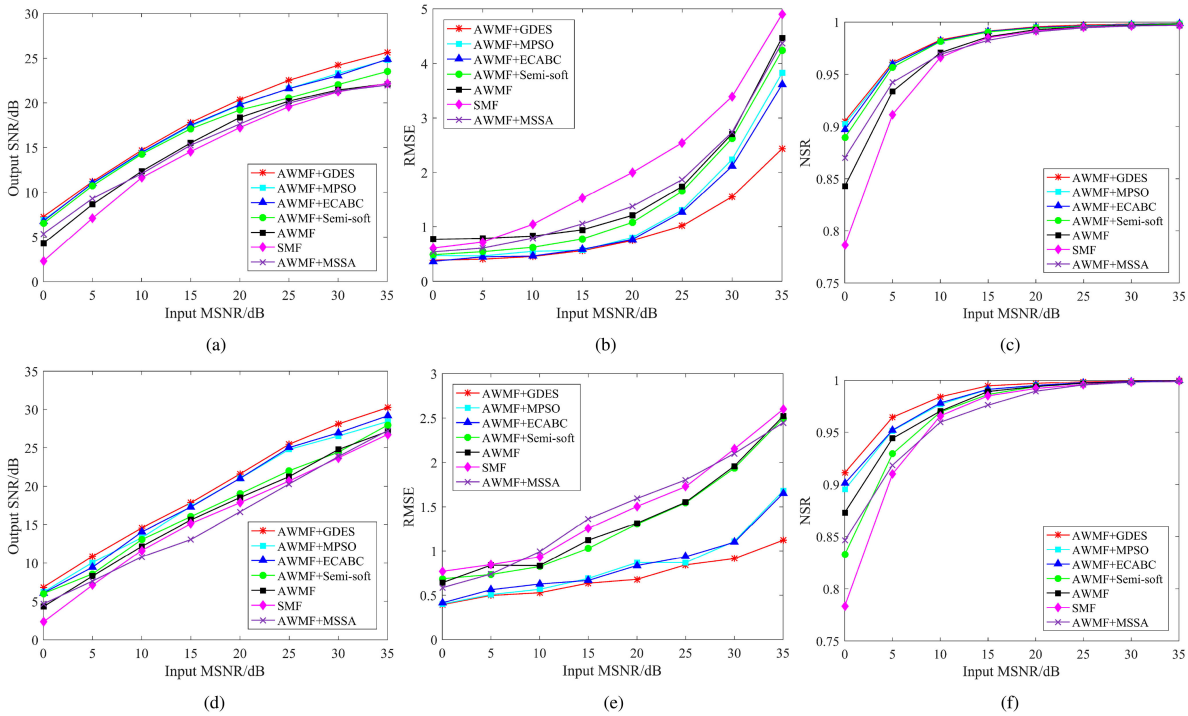

Fig. 11. Comparison of output SNRs, RMSEs, and NSRs as a function of the input MSNR (when input SNR = 5 dB) after denoising QPSK and 16QAM signals using 7 different algorithms. (a) Output SNR of QPSK. (b) RMSE of QPSK. (c) NSR of QPSK. (d) Output SNR of 16QAM. (e) RMSE of 16QAM. (f) NSR of 16QAM.

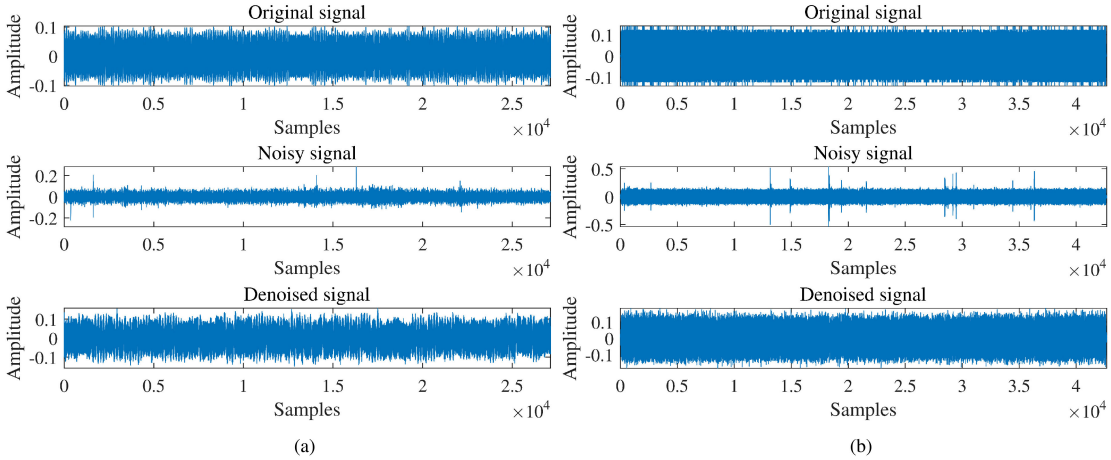

Fig. 12. Denoising of the BPSK signal collected during two sea trials using the proposed AWMF+GDES. (a) 60 m. (b) 120 m.

TABLE VI
COMPARISON OF OUTPUT SNRS, RMSES, AND NSRS OBTAINED BY DIFFERENT METHODS DURING TWO SEA TRIALS

Algorithms		SMF	AWMF	AWMF+Semi-soft	AWMF+MSSA	AWMF+MPSO	AWMF+ECABC	AWMF+GDES
60 m	Output SNR	17.5495	18.3554	18.5634	19.0424	14.8602	19.1144	**19.1234**
	RMSE	0.0038	0.0035	0.0034	**0.0032**	0.0052	**0.0032**	**0.0032**
	NSR	0.9933	0.9928	0.9932	0.9938	0.9836	0.9939	**0.994**
120 m	Output SNR	-1.4969	15.4045	2.7601	10.1603	15.4449	15.4387	**15.4872**
	RMSE	0.0917	0.0131	0.0557	0.0239	**0.013**	**0.013**	**0.013**
	NSR	-0.7738	0.9858	0.7246	0.9872	0.9856	0.9856	**0.988**

Therefore, all the algorithms obtained better performance due to the strong SOI, and the output SNR reached 17 dB. However, when the average distance between transducers was 120 m, the denoising performance of SMF and AWMF+Semi-soft dropped sharply, and even the reconstruction of the SMF algorithm failed. In addition, the optimized denoising algorithm is better than the non-optimized algorithm in terms of output SNR, RMSE, and NSR, which is consistent with the numerical simulation presented in Section IV. Thus, the algorithms proposed in this paper can obtain the best denoising performance. Overall, the obtained results show that the proposed underwater acoustic signal denoising algorithm can obtain a satisfactory performance for underwater acoustic signal denoising.

VI. Conclusion

In this paper, a novel underwater acoustic signal denoising method, named as AWMF+GDES, is proposed for Gaussian/non-Gaussian impulsive additive noise for underwater acoustic SISO channel. In the proposed method, the AWMF is used to suppress the non-Gaussian impulsive noise, and the wavelet threshold optimization algorithm based on GDES-ABC is used to suppress the Gaussian noise. The numerical simulations and the experimental results show that the proposed AWMF+GDES algorithm outperforms the existing algorithms and obtains a better performance. Overall, the proposed algorithm is able to achieve better denoising effect and retain the information of the original underwater acoustic signal than the other methods.

References

[1] Z. Q. Liu, "Combating impulsive noise for multicarrier underwater acoustic communications," *J. Acoustic. Soc. Amer.*, vol. 141, no. 5, pp. 3988–3988, May 2017.

[2] E. Zhang and A. Abdi, "Experimental results on synchronization with chirp signals using a vector sensor receiver," *J. Acoustic. Soc. Amer.*, vol. 141, no. 5, pp. 3915–3915, May 2017.

[3] A. Agrawal, R. Kumar, and M. Agrawal, "Modeling of underwater noise," in *Proc. OCEANS*, Marseille, France, Jun. 2019, pp. 1–6.

[4] R. Barazideh, W. S. Sun, B. Natarajan, A. Nikitin, and Z. H. Wang, "Impulsive noise mitigation in underwater acoustic communication systems: Experimental studies," in *Proc. IEEE 9th Annu. Comput. Commun. Workshop Conf.*, Las Vegas, NV, USA, Jan. 2019, pp. 0880–0885.

[5] S. C. Wang, Z. Q. He, K. Niu, P. Chen, and Y. Rong, "New results on joint channel and impulsive noise estimation and tracking in underwater acoustic OFDM systems," *IEEE Trans. Wireless Commun.*, vol. 19, no. 4, pp. 2601–2612, Jan. 2020.

[6] H. Q. Huang, J. C. Tang, B. Zhang, J. F. Chen, J. J. Zhang, and X. Song, "A novel nonlinear algorithm for non-Gaussian noises and measurement information loss in underwater navigation," *IEEE Access*, vol. 8, pp. 118472–118484, Jun. 2020, doi: 10.1109/ACCESS.2020.3004871.

[7] J. Chen and S. Guan, "Correntropy-based DOA estimation algorithm under impulsive noise environments," *EURASIP J. Wireless Commun. Netw.*, vol. 2020, no. 1, Jul. 2020, doi: 10.1186/s13638-020-01766-6.

[8] X. Yan, G. N. Liu, H. C. Wu, G. Y. Zhang, Q. Wang, and Y. Y. Wu, "Robust modulation classification over $\alpha-$stable noise using graph-based fractional lower-order cyclic spectrum analysis," *IEEE Trans. Veh. Technol.*, vol. 69, no. 3, pp. 2836–2849, Mar. 2020.

[9] M. Q. Liu, N. Zhao, J. F. Li, and V. C. M. Leung, "Spectrum sensing based on maximum generalized correntropy under symmetric alpha stable noise," *IEEE Trans. Veh. Technol.*, vol. 68, no. 10, pp. 10262–10266, Oct. 2019.

[10] E. Panayircl, H. Senol, M. Uysal, and H. V. Poor, "Sparse channel estimation and equalization for OFDM-based underwater cooperative systems with amplify-and-forward relaying," *IEEE Trans. Signal Process.*, vol. 64, no. 1, pp. 214–228, Jan. 2016.

[11] D. Middleton, "Non-gaussian noise models in signal processing for telecommunications: New methods an results for class A and class B noise models," *IEEE Trans. Inf. Theory*, vol. 45, no. 4, pp.1129–1149, May 1999.

[12] Y. C. Li, Y. Y. Wang, W. B. Yu, and X. P. Guan, "Multiple autonomous underwater vehicle cooperative localization in anchor-free environments," *IEEE J. Ocean. Eng.*, vol. 44, no. 4, pp. 895–911, Oct. 2019.

[13] G. Qiao, S. W. Gan, S. Z. Liu, and Q. J. Song, "Self-interference channel estimation algorithm based on maximum-likelihood estimator in in-band full-duplex underwater acoustic communication system," *IEEE Access*, vol. 6, pp. 62324–62334, Oct. 2018.

[14] X. B. Zhang, W. W. Ying, P. X. Yang, and M. Sun, " Parameter estimation of underwater impulsive noise with the class B model, IET radar, Sonar Navigation," vol. 14, no. 7, pp. 1055–1060, Jun. 2020.

[15] C. J. J. Sheela and G. Suganthi, "An efficient denoising of impulse noise from MRI using adaptive switching modified decision based unsymmetric trimmed median filter," *Biomed. Signal Process. Control*, vol. 55, Jan. 2020, doi: 10.1016/j.bspc.2019.101657.

[16] H. Kim, C. Jin, M. Kim, and K. Kim, "Damage detection of bottom-set gillnet using artificial neural network," *Ocean Eng.*, vol. 208, Jul. 2020, doi: 10.1016/j.oceaneng.2020.107423.

[17] V. R. Vijaykumar, M. G. Santhana, and D. Ebenezer, "Fast switching based median-mean filter for high density salt and pepper noise removal," *AEU - Int. J. Electron. Commun.*, vol. 68, no. 12, pp. 1145–1155, Dec. 2014.

[18] P. R. Chanu and K. M. Singh, "A two-stage switching vector median filter based on quaternion for removing impulse noise in color images," *Multimedia Tools Appl.*, vol. 78, no. 11, pp. 15375–15401, Jun. 2019.

[19] G. L. Wang, T. L. Li, G. Q. Zhang, X. G. Gui, and D. G. Xu, "Position estimation error reduction using recursive-least-square adaptive filter for model-based sensorless interior permanent-magnet synchronous motor drives," *IEEE Trans. Ind. Electron.*, vol. 61, no. 9, pp. 5115–5125, Sep. 2014.

[20] L. Boubchir and B. Boashash, "Wavelet denoising based on the MAP estimation using the BKF prior with application to images and EEG signals," *IEEE Trans. Signal Process.*, vol. 61, no. 8, pp. 1880–1894, Apr. 2013.

[21] J. L. Gu, P. R. Lin, B. W. K. Ling, C. Q. Yang, and P. H. Feng, "Grouping and selecting singular spectral analysis components for denoising based on empirical mode decomposition via integer quadratic programming," *IET Signal Process.*, vol. 12, no. 5, pp. 599–604, Jul. 2018.

[22] W. C. Kuang, S. J. Wang, Y. X. Lai, and W. Ling, "Efficient and adaptive signal denoising based on multistage singular spectrum analysis," *IEEE Trans. Instrum. Meas.*, vol. 70, Jul. 2020, doi: 10.1109/TIM.2020.3010426.

[23] S. Sardy, "Minimax threshold for denoising complex signals with waveshrink," *IEEE Trans. Signal Process.*, vol. 48, no. 4, pp. 1023–1028, May 2000.

[24] T. Xue, L. S. Xu, Q. Wang, B. Wu, and J. Huang, "A 3-D reconstruction method of dense bubbly plume based on laser scanning," *IEEE Trans. Instrum. Meas.*, vol. 69, no. 5, pp. 2145–2154, May 2020.

[25] R. Farhadiani, S. Homayouni, and A. Safari, "Hybrid SAR speckle reduction using complex wavelet shrinkage and non-local PCA-based filtering," *IEEE J. Sel. Top. Appl. Earth Observ. Remote Sens.*, vol. 12, no. 5, pp. 1489–1496, May 2019.

[26] D. L. Donoho and I. M. Johnstone, "Ideal spatial adaptation by wavelet shrinkage," *Biometrika*, vol. 81, no. 3, pp. 425–455, Sep. 1994.

[27] D. L. Donoho and I. M. Johnstone, "Adapting to unknown smoothness via wavelet shrinkage," *J. Amer. Statist. Assoc.*, vol. 90, no. 432, pp. 1200–1224, 1995.

[28] D. L. Donoho, "De-noising by soft-thresholding," *IEEE Trans. Inf. Theory*, vol. 41, no. 3, pp. 613–627, May 1995.

[29] T. H. Yi, N. H. Li, and X. Y. Zhao, "Noise smoothing for structural vibration test signals using an improved wavelet thresholding technique," *IEEE Trans. Image Process.*, vol. 12, no. 8, pp. 11205–11220, Aug. 2012.

[30] A. Sumithra and B. Thanushkodi, "Performance evaluation of different thresholding methods in time adaptive wavelet based speech enhancement," *IACSIT Int. J. Eng. Technol.*, vol. 1, no. 5, pp. 439–447, Dec. 2009.

[31] S. Singh, M. Tripathy, and R. S. Anand, "A wavelet packet based approach for speech enhancement using modulation channel selection," *Wirel. Pers. Commun.*, vol. 95, no. 4, pp. 4441–4456, Aug. 2017.

[32] S. M. Zhang, M. Zhang, Z. Q. Xu, and K. Wang, "Denoising algorithm for dual-tree complex wavelet disturbance signal with improved threshold function," in *Prco. 2020 Asia Energy Elect. Eng. Symp.*, Chengdu, China, May 2020, pp. 380–385.

[33] H. Sun and J. Zhao, "Shearlet threshold denoising method based on two sub-swarm exchange particle swarm optimization," in *Proc. IEEE Int. Conf. Granular Comput.*, San Jose, CA, USA, Aug. 2010, pp. 449–452.

[34] G. G. Bhutada, R. S. Anand, and S. C. Saxena, "PSO-based learning of sub-band adaptive thresholding function for image denoising," *Signal, Image Video Process.*, vol. 6, no. 1, pp. 1–7, Mar. 2012.
[35] C. He, J. C. Xing, J. L. Li, Q. L. Yang, and R. H. Wang, "A new wavelet thresholding function based on hyperbolic tangent function," *Math. Probl. Eng.*, vol. 2015, pp. 1–10, 2015.
[36] A. Kumar, N. Agrawal, I. Sharma, S. Lee, and H. N. Lee, "Hilbert transform design based on fractional derivatives and swarm optimization," *IEEE Trans. Cybern.*, vol. 50, no. 5, pp.2311–2320, May 2020.
[37] J. Qi, L. Li, Z. X. Shen, B. Xu, K. S. Leung, and Y. F. Sun, "Low-carbon community adaptive energy management optimization toward smart services," *IEEE Trans. Ind. Informat.*, vol. 16, no. 5, pp. 3587–3596, May 2020.
[38] C. Leboucher *et al.*, "An enhanced particle swarm optimization method integrated with evolutionary game theory," *IEEE Trans. Games*, vol. 10, no. 2, pp. 221–230, Jun. 2018.
[39] D. P. Kong, T. Q. Chang, W. J. Dai, Q. D. Wang, and H. Z. Sun, "An improved artificial bee colony algorithm based on elite group guidance and combined breadth-depth search strategy," *Inf. Sci.*, vol. 442, pp. 54–71, May 2018.
[40] X. Zhang, J. L. Li, J. C. Xing, P. Wing, Q. L. Yang, and C. He, "A particle swarm optimization technique-based parametric wavelet thresholding function for signal denoising," *Circuits, Systems, Signal Process.*, vol. 36, pp. 247–269, Apr. 2016.

Jingjing Wang (Member, IEEE) received the B.S. degree in industrial automation from Shandong University, Jinan, China, in 1997, the M.Sc. degree in control theory and control engineering from the Qingdao University of Science and Technology, Qingdao, China, in 2002, and the Ph.D. degree in computer application technology from the Ocean University of China, Qingdao, China, in 2012. She is a Professor with the School of Information Science and Technology, Qingdao University of Science and Technology. From 2014 to 2015, she was a Visiting Professor with the University of British Columbia. Her research interests include underwater wireless sensor network, underwater acoustic communications, ultra-wideband radio systems, and MIMO wireless communications.

Jiaheng Li received the master's degree in computer science and technology from the Qingdao University of Science and Technology, Qingdao, China, in 2020. He is currently working toward the Ph.D. degree with the Xiamen University, Xiamen, China. He is a Reviewer of IEEE TRANSACTIONS ON VEHICULAR TECHNOLOGY. His current research interests include underwater acoustic communications, array signal processing, and optimization theory.

Shefeng Yan (Senior Member, IEEE) received the B.Sc., M.Sc., and Ph.D. degrees from Northwestern Polytechnical University, Xi'an, China, in 1999, 2001, and 2005, respectively, all in electrical engineering.

He was a Postdoctoral Research Associate with the Institute of Acoustics, Chinese Academy of Sciences (IACAS), Beijing, China, from 2005 to 2007, and with the Department of Electronics and Telecommunications, Norwegian University of Science and Technology, Trondheim, Norway, from 2007 to 2009, respectively. He was a Senior Visiting Scholar with the Department of Electrical, Electronic and Communication Engineering, University of Erlangen-Nuremberg, Erlangen, Germany, from December 2015 to February 2016. Since 2009, he has been a Professor with IACAS, and with the University of Chinese Academy of Sciences. He has authored the book *Broadband Array Processing* (Springer, 2019). His research interests include acoustic signal processing, statistical and array signal processing, and underwater acoustic communications.

Prof. Yan is a member of the Acoustical Society of America. He was the recipient of the 2010 ICA-ASA Young Scientist Grant for excellent contributions to Acoustics and a co-recipient of the Best Paper Awards at SENSORCOMM 2008, WASPAA 2009, and WCSP 2018.

Wei Shi received the B.S. degree from Ludong University, Yantai, China, in 2009, the master's degree in signal and information processing from the Ocean University of China, Qingdao, China, in 2011, and the Ph.D. degree in computer application technology from the Ocean University of China, Qingdao, China, in 2014. Since 2014, he has been a Lecturer with the College of Information Science and Technology, Qingdao University of Science and Technology. His research interests include underwater wireless sensor network, OFDM, MIMO, LTE, UWB, 60 GHz wireless communications, cooperative communication networks and indoor positioning.

Xinghai Yang (Member, IEEE) is currently an Associate Professor with the School of Information Science and Technology, Qingdao University of Science and Technology, Qingdao, China. He received the B.S. degree in electronic information science and technology, the M.D. degree in communication and information system, and the Ph.D. degree in communication and information system from Shandong University, China, in 2000, 2003, and 2011, respectively. From 2015 to 2016, he worked as a Visiting Professor with University of British Columbia, Canada. His current research interests include underwater acoustic signal processing, deep learning, wireless communications, and Internet of Things.

Ying Guo received the B.E. degree from the Qingdao University of Science and Technology in 2007. She received the Ph.D. degree from the Department of Computer Science and Technology, Ocean University of China, in 2010. She is an Associate Professor with the Qingdao University of Science and Technology, and a Visiting Scholar in Arizona State University. Her research interests include wireless sensor networks, underwater acoustic networks, and Internet of Things.

T. Aaron Gulliver (Senior Member, IEEE) received the Ph.D. degree in electrical and computer engineering from the University of Victoria, Victoria, BC, Canada, in 1989. From 1989 to 1991, he was employed as a Defense Scientist with Defense Research Establishment Ottawa, Ottawa, ON, Canada. He has held academic positions with Carleton University, Ottawa, and the University of Canterbury, Christchurch, New Zealand. He joined the University of Victoria in 1999 and is a Professor with the Department of Electrical and Computer Engineering. In 2002, he became a Fellow of the Engineering Institute of Canada, and in 2012 a Fellow of the Canadian Academy of Engineering. His research interests include information theory and communication theory, and ultra-wideband communications.